THE ASTROPHYSICAL JOURNAL, 340:679–697, 1989 May 15

EXTRAGALACTIC JETS AS CURRENT CARRYING SYSTEMS. II. MAGNETOHYDRODYNAMIC TURBULENCE, RELATIVISTIC ELECTRON DISTRIBUTION, AND OBSERVABLE QUANTITIES

EDVIGE CORBELLI
Osservatorio Astrofisico di Arcetri

AND

PIERLUIGI VELTRI
Dipartimento di Fisica, Universita' della Calabria
Received 1988 June 20; accepted 1988 September 28

ABSTRACT

Relativistic electrons in extragalactic radio jets could act as tracers of only a restricted area of a magnetic field generated by the current structure. In the present paper we present a model for a conical distribution of relativistic electrons inside a cylindrical thermal jet which obeys the MHD model of Chiuderi, Pietrini, and Torricelli-Ciamponi (1989). Two different geometries are explained on the basis of stochastic diffusion of the relativistic particles on the field lines. This diffusion is shown to be a consequence of the properties of the MHD turbulence which develops in the jet.

Model predictions for intensity profiles, degree of polarization, and apparent magnetic field configurations are shown, and many of them are in good agreement with observed radio jet structures.

Subject headings: galaxies: jets — hydromagnetics — polarization

I. INTRODUCTION

It is commonly accepted that the observed radio emission from extragalactic radio jets is produced by synchrotron mechanism. This mechanism requires the presence of magnetic fields and relativistic electrons in jets (Ginzburg and Syrovatskii 1965; Pacholczyk 1970). Polarization measurements in jets show that the apparent magnetic field, viz. the projection of the three-dimensional field on the plane of the sky, is organized in highly ordered structures. In particular, in the most powerful sources, where one-sided jets are commonly observed, this field seems to be uniformly parallel to the jet axis, whereas in weaker sources the magnetic field displays a more structured behavior (NGC 6251; Perley, Bridle, and Willis 1985; NGC 315, Willis *et al.* 1981; 3C 31, Fomalont *et al.* 1980; 3C 465, van Breugel 1980). The most common apparent magnetic field configurations can be summarized as follows:

1) Apparent field predominantly parallel to the jet axis;
2) Apparent field predominantly perpendicular to the jet axis;
3) Perpendicular apparent field in the center of the jet and longitudinal at the edges;
4) Longitudinal apparent field near the core and perpendicular further out;
5) A few regions of oblique apparent field or more complex structures near the end of the jet.

Configurations (3), (4), and (5) imply varying internal structures as the distance from the nucleus increases. From this, many authors have argued that the tri-dimensional magnetic field itself varies longitudinally. In fact, if there is a flux-conserving expansion of the jet, and the magnetic field is transported along with the relativistic electron beam, the field component parallel to the jet axis varies as $B_{\parallel} \propto R^{*-2}$, while for the perpendicular component we should have $B_{\perp} \propto R^{*-1}$ (Blandford and Rees 1974), where R^* is the radius of the radio-emitting region.

These variations cannot explain all the apparent magnetic field structures other than configuration (4) in a satisfactory way. Also, if there is a particle flux conservation along the jet, they predict very steep laws for the luminosity evolution from the core to the outermost jet regions. In the most favorable case, in which the radiating particles do not work in lateral expansion, $I \propto NR^*B_{\perp}^{(\gamma+1)}$, where γ is the spectral index of the synchrotron spectrum. The intensity for this model will then scale at least as fast as $R^{*-2.6}$. Magnetic field amplification (De Young 1982) or particle reacceleration (Henriksen, Bridle, and Chan 1982) is required to account for the discrepancy between the observed brightness variation ($I \propto R^{*-t}$, $1.2 < t < 1.6$ [Bridle and Perley 1984], except in regions very distant from the core) and those predicted using the $B_{\perp} \propto R^{*-1}$ law. Other observed radio jet properties we want to point out concern the radial and longitudinal variations of the degree of polarization, the small average opening angle of the radio-emitting region, and the decrease of its expansion rate as we go far from the galactic nucleus (see Bridle and Perley 1984; Begelman, Blandford, and Rees 1984 for a review).

Attempts to fit the total and polarized intensity have sometimes been made by explicit calculation of the Stokes parameters for a given model (Laing 1981; Königl and Choudhuri 1985). For example, Laing (1981) calculated the predicted intensity and polarization for the helical and CH (Chan and Henriksen 1980) models and showed that there are several problems in fitting the observations.

There is a big controversy about the importance of thermal matter, magnetic fields, and mass flow in setting the jet in equilibrium with the environment. But, as it has been pointed out in the paper by Chiuderi, Pietrini, and Torricelli-Ciamponi (1989, hereafter Paper I), using the equipartition hypothesis for the energy density of magnetic fields and relativistic electrons, $E_B \sim E_r$, and depolarization measurements to estimate the mean thermal electron density (Perley, Willis, and Scott 1979; Willis *et al.* 1981; van

Breugel 1980), it is reasonable to believe that the thermal matter gives the main contribution to the currents which generate the magnetic field. Current models in a jet can then be set up independently from a detailed knowledge of the relativistic electron distribution. In the following we will use the current model proposed and discussed in Paper I to study a possible distribution of relativistic electrons inside it.

In Paper I it was also shown that the occurrence of MHD instabilities in cylindrical magnetic structures is a rather common phenomenon. These instabilities could produce a certain level of MHD turbulence fluctuations, which can considerably affect the relativistic electron distribution function. In particular, if we suppose that the relativistic component of the jet is injected in a small region near the core of the radio galaxy, the relativistic electrons could diffuse following the fluctuations of the field lines (Jokipii 1966; Benford, Ferrari, and Trussoni 1981), thus producing a distribution of more or less conical shape. Moving away from the core, relativistic electrons light up wider and wider zones of the current region showing longitudinal variations in the structure of the apparent magnetic field. Using this model, since the magnetic field and the relativistic electron region are not coincident over the whole jet structure, we will be able to avoid some of the difficulties in explaining observational data mentioned above. For example, in order to explain the slow decrease in luminosity, the model which we will discuss does not necessarily need particle reacceleration or magnetic field amplification over the whole jet, even if the existence of local phenomena of particle reacceleration is not excluded. Also, if diffusion is responsible for the widening of the radio-emitting region, the observed decrease of the opening angle far from the core is naturally explained. Notice that acceleration and diffusion theory on MHD fluctuations predicts relativistic electrons traveling outward from the core along the field lines, and this gives a reasonable explanation of the one-sidedness phenomenon.

It is worthwhile noting that in order to set up the picture we have just outlined in a coherent way, we have to suppose that the relativistic electrons do not affect the dynamics of the jet and serve merely as tracers of the underlying structure. Then the energy density (or equivalently the pressure) of the relativistic component must be negligible with respect to the contribution of the thermal component and magnetic field. However, in the introduction of Paper I it has been pointed out that the assumption of a magnetic field B slightly bigger than its equipartition value results in a small ratio E_r/E_B. Because of the uncertainty in the estimate of B we can safely conclude that the unbalance between magnetic and thermal energy, on one side, and relativistic particles, on the other, cannot be ruled out, neither on theoretical nor on observational grounds.

The plan of the paper is the following: in § II we discuss the expected properties of MHD turbulence, on the basis of what is actually known both from theoretical considerations and from solar wind observations. In § III, with the analysis of the acceleration and diffusion mechanisms for the relativistic electrons on MHD turbulence fluctuations, we justify the choice of considering different structures for the radio-emitting and the current region. We carry out in § IV an explicit calculation of the Stokes parameters for our model. Finally, in § V we emphasize the model predictions on observable properties such as collimation, apparent magnetic field structures, degree of polarization, and intensity profiles. We also try to fit with our model some of the best resolved jets.

II. MHD TURBULENCE CHARACTERIZATION

It is commonly accepted that turbulence develops in a MHD structure characterized by a high Reynolds number, like a jet (De Young 1980; Henriksen, Bridle, and Chan 1982). Such turbulence is usually invoked to accelerate the relativistic electrons necessary to explain the observed synchrotron emission (Lacombe 1977). Moreover, it has been proposed by Benford, Ferrari, and Trussoni (1980) that MHD turbulence might also explain the widening of the jets as due to relativistic electron diffusion on turbulent fluctuations. In order to understand what could be the effects of MHD turbulence on electron acceleration and diffusion, we discuss the expected characteristics of this turbulence in this section. The primary sources of MHD turbulence are the linear instabilities which may start developing on large scales (of the order of the jet radius). Some of these instabilities have been studied in Paper I, but others, such as Kelvin-Helmholtz instabilities when there is mass flow, might be present as well. A detailed analysis of what happens in a jet due to the occurrence of such instabilities would require a detailed knowledge of the characteristics of all such instabilities. However, some qualitative considerations and estimates can be made.

The turbulence starts developing at wavelengths where linear instabilities are present, usually called the injection domain. When the energy density level in the fluctuations produced by the instabilities becomes sufficiently high, non-linear interactions between modes at different wavelengths are important. In the theory of strong and incompressible MHD turbulence, which develops in a three-dimensional structure, it is well known that these nonlinear interactions produce an energy cascade toward smaller and smaller wavelengths, i.e., toward large wave vectors (De Young 1980; Grappin *et al.* 1982; Matthaeus and Montgomery 1984; Pouquet *et al.* 1986). Then energy spectra in plasmas with high Reynolds numbers will extend over many wavelength decades. The cutoff of these energy spectra is localized at wavelengths where the dissipation mechanism is more efficient than the nonlinear energy transfer, and this is the so-called dissipation domain. Finally, the region of the spectrum where neither injection nor dissipation is present is called the inertial domain. Here spectral indices of the Kolgomorov's (5/3) or Kraichnan's (3/2) type are expected for the energy density in the waves.

When the turbulent energy injection due to the instabilities is balanced by the nonlinear energy transfer toward smaller wavelengths, a stationary state can be achieved. In such a case, if we divide the magnetic field into its average and fluctuating part,

$$\boldsymbol{B} = \boldsymbol{B}_0 + \delta\boldsymbol{B} ,$$

an order-of-magnitude estimate for the level of turbulent fluctuations can be obtained by equating estimates of linear and nonlinear terms, which control the turbulent energy density evolution. Namely, while the rate of linear injection of energy due to an instability with growth rate ν is of the order of $\nu\,\delta W \propto \nu\langle\delta B^2\rangle$, δW being the energy density in the fluctuations, the rate of the nonlinear cascade is roughly proportional to $\langle\delta B^2\rangle^2$. The two processes are then balanced when

$$\nu\tau_A \sim \frac{\delta W}{B_0^2} \approx \frac{\langle\delta B^2\rangle}{B_0^2} \tag{2.1}$$

(Carbone, Einaudi, and Veltri 1987), where $\tau_A = R/v_A = R(4\pi\rho)^{1/2}/B_0$ is a typical Alfvén time for a medium with mass density ρ and typical dimension R. If ν is the maximum growth rate of the instabilities in equation (2.1), we can see that when $\nu\tau_A$ is smaller than unity, the energy level in MHD fluctuations remains small compared to the energy density in the ordered magnetic field. In such case we can assume that the effect of the instabilities is not to destroy the structure but only to produce a certain amount of turbulence carrying energy toward small wavelengths. When, on the contrary, $\nu\tau_A \geq 1$, the instabilities are expected to destroy the ordered magnetic field structure. We will limit the following analysis to models which do not have such fast-growing instabilities and will keep magnetic field fluctuations down to low levels. As it has been found for the ideal magnetic instabilities in Paper I, we expect the instabilities to grow faster as the azimuthal component of the magnetic field increases. Models with a small azimuthal component of the magnetic field, for which the maximum growth rate of the instabilities is smaller than $1/\tau_A$, should then be considered in the jet for the ordered large-scale structure of the magnetic field to be preserved. This seems also to be the case when a nonrelativistic mass flow is considered in the thermal structure (Pietrini and Torricelli-Ciamponi 1989).

A completely different view of the mechanism for MHD turbulence production has been proposed by Eilek (1979). In that picture a spectrum of Alfvén wave turbulence is produced totally through the balance between an energy injection, due to a Kelvin-Helmholtz instability and proportional to the modulus of the wave vector, k, and an energy damping rate, due to the absorption of the waves by the relativistic electrons and proportional to $k^{-3/2}$. The energy spectrum for relativistic electrons is assumed to be $\propto E^{-2.5}$ (where E is the energy of the electrons). The strong absorption by relativistic electrons prevents the nonlinear interaction between Alfvén waves. As a result, a turbulence spectrum proportional to $k^{-1/2}$ can be obtained. However, we think that the hypotheses required to set up this picture are hardly recovered in a jet. First of all, a Kelvin-Helmholtz instability cannot be expected to produce an energy injection proportional to k on length scales ranging from 10^{22} cm (the jet radius) up to 10^9 cm (the energy cutoff due to absorption on thermal electrons). Also, let us consider the resonant condition between waves of frequency ω and electrons with energy E, cyclotron frequency Ω, and velocity component parallel to the field, $v_\parallel$:

$$\omega - n\Omega^* - k_\parallel v_\parallel = 0 \tag{2.2}$$

(where $\Omega^* = \Omega m_e c^2/E$, $k_\parallel$ is the component of the wave vector parallel to the magnetic field, and n is some integer; Melrose 1968). When the relativistic electron Larmor radius is much smaller than the perpendicular wavelength, $(k_\perp c)/\Omega^* \ll 1$, the electrons have a nonzero wave absorption coefficient only for $n = -1$ (Melrose 1980). In such a case we can notice that in order to have an efficient resonant interaction between relativistic electrons and Alfvén wave turbulence up to wavelengths of the order of 10^{22} cm, as supposed by Eilek, we need to have relativistic electrons with energy up to 10^{21} eV, and there are no observations which indicate the presence of electrons with such high energies in jets (as a comparison, we recall that the energy required to produce X-rays through the synchrotron emission mechanism is $\sim 10^{14}$ eV).

If we suppose instead that the energy of relativistic electrons ranges from 10^{10} eV (radio) to 10^{14} eV (X-rays), the relativistic electrons would interact resonantly only with wavelengths ranging from 10^9 to 10^{11} cm. This in turn means that the presence of relativistic electrons could modify the usual picture of MHD turbulence, as produced by nonlinear wave-wave interactions, only in a short-wavelength range, where interactions with relativistic electrons might be considered the main energy sink (Lacombe 1977). It is also worth noting, as pointed out by Barnes (1978), that magnetosonic waves are strongly damped by a thermal electron gas (this explains, for example, the absence of compressible fluctuations in the solar wind). As a consequence of what we have just discussed, in our jet model where a thermal electron gas is present, the turbulence in the large-wavelength range 10^{11}–10^{22} cm is expected to be both hydrodynamic and incompressible in nature, much the same as the turbulence in the solar wind.

This situation is fortunate since the solar wind represents perhaps the best studied example of MHD turbulence from an observational point of view (Coleman 1968; Belcher and Davis 1971). Huge progress in our understanding of incompressible MHD turbulence has been made in recent years, owing to both theoretical calculations performed by solving evolution equations for average turbulent quantities based on closure hypothesis (eddy-damped quasi-normal Markovian approximation, direct interaction approximation, etc.), and also to direct numerical simulations of Navier-Stokes equations.

It has now been firmly established, as shown by Livshits and Tsytovich (1970) in the framework of weak turbulence, that strong isotropic MHD turbulence evolves naturally toward a state where, of the two Alfvén wave modes propagating in a magnetic field, only one survives, viz. the one that initially dominates (Dobrowolny, Mangeney, and Veltri 1981; Grappin *et al.* 1982; Matthaeus and Montgomery 1984; Pouquet, Meneguzzi, and Frish 1986). This in turn means the following:

1. Velocity and magnetic field fluctuations are strongly correlated:

$$\delta v = \sigma \frac{\delta B}{\sqrt{4\pi\rho}},$$

where $\sigma = 1$ if the surviving mode is the one propagating in the direction of the magnetic field and $\sigma = -1$ in the opposite case.

2. Only one sign for the parallel component of the wave vectors is present: i.e., either $k_\parallel > 0$ (if the waves propagate in the direction of the magnetic field) or $k_\parallel < 0$ (if the waves propagate in the opposite direction). This result will be shown to be of considerable interest in the theory of turbulent electron acceleration.

More recently these results have been extended to anisotropic situations. In particular, it has been demonstrated, both in two-dimensional simulations (Shebalin, Matthaeus, and Montgomery 1983) and in calculations of MHD turbulence evolution (Carbone and Veltri 1987, 1988), that the MHD turbulence spectrum is dominated by wave vectors perpendicular to the average magnetic field in the inertial range, the opposite situation occurring in the injection domain, i.e., for very large wavelengths.

An explicit model for the energy spectrum in the wave vector space can be set up. We have shown in Appendix A that, assuming statistical homogeneity and cylindrical symmetry around the mean magnetic field, the following expression for the correlation

tensor of the magnetic field fluctuations may be obtained:

$$\langle \delta B_i(\boldsymbol{r}, t)\delta B_j(\boldsymbol{r}, t)\rangle = 2\pi \int_0^\infty k_\perp \, dk_\perp \int_{-\infty}^{\infty} U_{ij}(k_\perp, k_\parallel) dk_\parallel \, , \tag{2.3}$$

with $U_{ij}(k_\perp, k_\parallel)$ the spectral correlation tensor, which, in a frame with the z-axis pointing in the direction of the mean magnetic field $\boldsymbol{B}_0$, is given by

$$\begin{pmatrix} U_\perp(k_\perp, k_\parallel)/2 & 0 & 0 \\ 0 & U_\perp(k_\perp, k_\parallel)/2 & 0 \\ 0 & 0 & U_\parallel(k_\perp, k_\parallel)/2 \end{pmatrix}. \tag{2.4}$$

In the same Appendix it is also shown that both $U_\perp(k_\perp, k_\parallel)$ and $U_\parallel(k_\perp, k_\parallel)$ may be expressed in terms of a single function $U(k_\perp, k_\parallel)$ as follows:

$$U_\parallel(k_\perp, k_\parallel) = \frac{k_\perp^2}{2k^2} U(k_\perp, k_\parallel) \, , \tag{2.4a}$$

$$U_\perp(k_\perp, k_\parallel) = \frac{k_\perp^2 + 2k_\parallel^2}{2k^2} U(k_\perp, k_\parallel) \, . \tag{2.4b}$$

By looking at the results of turbulence calculations of Carbone and Veltri (1988) we see that, at least in the inertial domain, the turbulence spectrum can be safely represented by

$$U(k_\perp, k_\parallel) = \frac{C}{(\lambda_\perp^2 k_\perp^2 + \lambda_\parallel^2 k_\parallel^2 + 1)^{(\alpha/2)+1}} \, , \tag{2.5}$$

where α is the usual spectral index ($\alpha > 1$), while $\lambda_\perp$ and $\lambda_\parallel$ are the perpendicular and parallel correlation lengths, respectively. In an isotropic medium $\lambda_\perp$ and $\lambda_\parallel$ are equal. On the contrary, in presence of a mean magnetic field $\lambda_\parallel \approx 2\lambda_\perp$ (Carbone and Veltri 1988; Shebalin, Matthaeus, and Montogomery 1983). The expression we have given is not valid in the injection or dissipation domains, but, as long as quantities integrated on the spectrum are considered, using such a formula we introduce an error which may be estimated to be on the order of

$$\max \{(k_D/k_I)^{1-\alpha}, (\lambda_\parallel k_I)^{2-\alpha}\} \, ,$$

where k_I and k_D are wave vectors typical of the injection and dissipation domains respectively ($k_D \sim 2\pi \times 10^{-11}$ cm^{-1}, $k_I \sim 2\pi \times 10^{-22}$ cm^{-1}). Since in our case we have

$$k_D \gg k_I \qquad \text{and} \qquad \lambda_\parallel k_I \ll 1 \, ,$$

we can safely assume expression (2.5) over the whole spectrum when calculating, for example, the average density in the fluctuating field:

$$u_B = \frac{\langle \delta B^2 \rangle}{8\pi} = \frac{1}{4} \int_0^\infty k_\perp \, dk_\perp \int_{-\infty}^{\infty} \frac{C}{(\lambda_\perp^2 k_\perp^2 + \lambda_\parallel^2 k_\parallel^2 + 1)^{(\alpha/2)+1}} \, dk_\parallel \, ,$$

thus obtaining

$$C = \frac{(\alpha - 1)\Gamma(\alpha/2 + 1)}{\sqrt{\pi}\,\Gamma(\alpha/2 + 0.5)} \lambda_\perp^2 \lambda_\parallel u_B \, , \tag{2.6}$$

$\Gamma(\alpha/2 + 1)$ and $\Gamma(\alpha/2 + 0.5)$ being the usual gamma functions.

III. ELECTRON ACCELERATION AND DIFFUSION

Let us discuss how the characteristics of MHD turbulence, which we have outlined in the previous section, influence electron acceleration and diffusion. Two basically different mechanisms for electron acceleration in presence of MHD turbulence might be at work:

1) The resonant acceleration;
2) The stochastic Fermi acceleration.

The resonant acceleration has been discussed extensively by Lacombe (1977) using results found previously by Melrose (1968). In Lacombe's paper the condition for such acceleration, sufficient to compensate for the synchrotron losses, is discussed. However, the resonance condition (eq. [2.2]) requires particles with energy at least on the order of 10^{10} eV to be satisfied. A primary acceleration mechanism is then necessary to bring the electrons to such high energies. In the following we do not investigate such a mechanism, but we suppose only that the primary acceleration mechanism takes place near the core of the radio galaxy.

There is an extremely interesting consequence to such a picture: first of all, if the relativistic particles are ejected from the core of the galaxy, the relativistic electrons propagate along the magnetic field only in one direction: they move outward from the core to the radio lobes. This direction is also that of propagation of Alfvén waves which survive the nonlinear cascade production: i.e., only $k_\parallel$ corresponding to outward propagation is present in turbulence. Now, if we recall the semiclassical approach in the theory of

interaction of waves and particles (Melrose 1968), electron acceleration requires absorption of a photon by the particles. In such elementary process, the parallel momentum conservation implies that the electron parallel momentum after absorption is

$$p'_{\parallel} = p_{\parallel} + \hbar k_{\parallel} .$$

The implies that if $p_{\parallel}$ and $k_{\parallel}$ have the same sign, the parallel momentum is increased in modulus. The mechanism of acceleration is not able to reverse the sign of the component of the electron momentum parallel to the magnetic field. We expect then a distribution of relativistic electron velocities where only one sign of $p_{\parallel}$ is present: that corresponding to outward propagation. It is also worth noting that the isotropization in pitch angles, which is a much faster mechanism than acceleration [by a factor $(c/v_A)^2$; Melrose 1968; Lacombe 1977], has to satisfy the same elementary conservation laws. It would not be able to isotropize particles over all the pitch angles, but only in the half-space where particles have a velocity component parallel to the background magnetic field, directed outward.

Let us consider now the Fermi acceleration on Alfvén waves. Explicit calculations by Skilling (1975) show that the efficiency of such a mechanism is much the same as that of the resonant acceleration discussed above, when both the wave propagation modes are present in the turbulence with almost the same energy densities. Otherwise the characteristic time for Fermi acceleration is increased by a factor which is roughly the ratio between the energy density of the stronger mode and the energy density of the weaker one. For this reason this mechanism is hardly thought to be at work when our picture of the MHD turbulence settles in a jet.

The main consequence of this is the fact that, if relativistic electrons are generated near the injection point of the jets, they propagate outward and the MHD turbulence eventually compensates for synchrotron losses. In such a case MHD turbulence may also play a role in setting up the spatial distribution of relativistic electrons. The relativistic particles streaming from the core to the lobes, in the drift approximation, follow the magnetic field lines and are subject to spatial diffusion perpendicular to the background magnetic field because of the random walk of the magnetic field lines (Jokipii 1966). As pointed out by Melrose (1980), such a diffusion mechanism is more efficient than resonant diffusion when the gyroradii of the particles are much smaller than the turbulence correlation length. This is certainly the case if MHD turbulence is generated by large-scale instabilities, as we have assumed, since in that case the correlation length is expected to be on the order of the jet radius. The explicit expression for the diffusion coefficient D perpendicular to the average magnetic field $\boldsymbol{B}_0$ can be found in Jokipii (1966) (see also Melrose; Zimbardo, Veltri, and Malara 1984):

$$D = \frac{v_{\parallel}}{B_0^2} \pi^2 \int_0^{\infty} k_{\perp} \, dk_{\perp} \int_0^{\infty} U_{\perp}(k_{\perp}, k_{\parallel}) \delta(k_{\parallel}) dk_{\parallel} ,$$

$v_{\parallel}$ being the particle velocity along the magnetic field. Using the expression (2.5) for the turbulent spectrum, a straightforward calculation gives

$$D = \frac{\sqrt{\pi}}{8} \frac{\alpha - 1}{\alpha} \frac{\Gamma(\alpha/2 + 1)}{\Gamma(\alpha/2 + 0.5)} \frac{\langle \delta B^2 \rangle}{B_0^2} \lambda_{\parallel} v_{\parallel} . \tag{3.1}$$

The possibility of such a diffusion had also been examined previously by Eilek (1979). However, in that analysis it was assumed that:

i) Only waves having $k = 0$ (and not $k_{\parallel} = 0$) contribute to the diffusion;

ii) The wave spectrum, necessary in order to estimate the energy level on waves at $k = 0$, is of the form $k^{-1/2}$.

The resulting diffusion coefficient is smaller than ours by a factor $(k_I/k_D)^{1/2}$, which in a jet may be as high as 10^6.

Bendford, Ferrari, and Trussoni (1980) have obtained more positive results in their attempt to explain jet morphology by assuming relativistic electron cross-field diffusion. They studied a relativistic electron beam which develops an extended profile (and thus a large synchrotron envelope), while most of the beam energy and momentum are carried in a narrower, proton-dominated beam. We are not interested in reconsidering detailed morphological effects of diffusion; rather, we will try to understand (§§ IV and V) what are the effects of relativistic electron diffusion, inside a more extended cylindrical magnetic field structure, on the total and polarized intensity of synchrotron emission.

For the moment we will limit ourselves to observe that an order-of-magnitude estimate for the widening angle of the jets may be obtained by recalling that the increase in the electron beam radius Δr due to cross field diffusion is related to D by

$$(\Delta r)^2 \approx 2D \frac{L}{v_{\parallel}} \tag{3.2}$$

(L being the length of the relativistic electron path since they were injected in the jet). The average jet opening $\Delta\beta$ may then be estimated, apart from numerical factors of the order unity, as

$$\Delta\beta \approx \frac{\Delta r}{L} \approx \sqrt{\frac{\lambda_{\parallel}}{L} \frac{\langle \delta B^2 \rangle}{B_0^2}} . \tag{3.3}$$

It can easily be seen that, assuming $\lambda_{\parallel}$ of the order of the jet radius, fluctuation levels of $\langle \delta B^2 \rangle / B_0^2 \approx 0.1$ are sufficient to explain all the observed widening of the jets. From equation (3.2) we notice that relativistic electron diffusion grows only with the square root of the path length along the jet, at least when the turbulent fluctuation level remains constant along the jet. On the other hand, as equation (2.1) indicates, the balance between linear instability and nonlinear wave interactions is such to maintain a more or less constant fluctuation level.

This diffusion seems, then, fairly well suited to explain the observed decreasing expansion rate of radio jets and especially the property that jets with orthogonal apparent magnetic fields are less collimated. This is not only due to the longer path electrons

have to follow in leaving the core but also to the higher level of fluctuations related to the presence of an azimuthal magnetic field. The level of fluctuations is in fact directly related to the instability growth rate, which in our model increases by increasing the magnetic field pitch angle (Paper I). As a consequence, we expect that higher values of the opening angle of a jet, which is a measure of the MHD fluctuation level, must be related to regions of orthogonal magnetic field.

Equation (3.1) for the diffusion coefficient is valid only when Coulomb collisions can be safely neglected. This is certainly the case for relativistic electrons. On the contrary, when thermal electrons are considered, it can be seen that the mean free path can be estimated as

$$\lambda_{\rm th} \approx \frac{v_{\rm th}}{\nu_C} \approx 0.2 \text{ kpc}$$

($v_{\rm th}$ being the electron thermal velocity and ν_C the Coulomb collision frequency). In this case the diffusion coefficient is reduced by the presence of collisions by a factor

$$\frac{h\lambda_{\rm th}}{\ln(\lambda_{\parallel}/r_L)}$$

(Rechester, Rosenbluth, and White 1979; Zimbardo, Veltri, and Malara 1984), where h is the Kolmogorov entropy and r_L is the thermal electron Larmor radius. By using the estimate

$$h \approx \frac{\langle \delta B^2 \rangle}{\lambda_{\parallel} B_0^2}$$

(Zimbardo *et al.* 1984), it can be shown that the diffusion coefficient for thermal electrons is reduced by a factor of the order of 10^{-2}. The diffusion rate of thermal electrons is then negligible in comparison with that of relativistic electrons, both because they are slower at least by a factor 10^{-1} and because collisions retard considerably the process of stochastic diffusion.

On the basis of what we have just shown, in the next section we will set up a model for the beam of relativistic electrons, inside a cylindrical thermal structure, with the following characteristics:

i) A more or less conical shape in space;

ii) A velocity distribution function where only particles are present which have the component of the momentum parallel to the average magnetic field, such that they propagate forward, away from the core.

We will then calculate the Stokes parameters for synchrotron radiation associated with such distribution and compare our results with observations.

IV. BRIGHTNESS AND POLARIZATION DISTRIBUTION

To test the validity of a model we should examine what are its predictions on observable quantities. We already mentioned in the previous sections how the development of turbulence on an MHD equilibrium and a stochastic diffusion process for collisionless particles gives a natural explanation to properties such as the decreasing expansion rate of the radio-emitting region or the anisotropic behavior of the radiating particle distribution with respect to the field lines. We now want to calculate explicitly the total intensity, the degree, and position angle of linear polarization predicted by our model using the MHD equilibrium given in Paper I.

As we have mentioned in the introduction, the observed degree of polarization and Faraday measurements are consistent with the presence of thermal matter, in and out of the radio-emitting region. The thermal particle density ($n_{\rm th}^e \approx 10^{-3}$–$10^{-4}$ cm^{-3}; Fanti 1983) is sufficiently high to give the main contribution in setting the current structure and the pressure profile. We recall that the basic picture of the equilibrium model comes from the requirement that the longitudinal current has a return path inside the jet walls. The current configuration considered in Paper I is

$$\boldsymbol{j}(r) = j_1[A(2-3\zeta)\theta(1-\zeta)\boldsymbol{e}_z + \zeta\theta(1-\zeta)\boldsymbol{e}_\theta] ,$$

where $\zeta = r/R$, $A = j_0/j_1$, R is the current region radius, j_0 and j_1 are constants [$j_0 = j_z(R)$, $j_1 = j_\theta(R)$], and $\theta(\zeta)$ is the Heaviside function. The magnetic field corresponding to this current distribution has a radially varying pitch angle and is

$$\boldsymbol{B}(\zeta) = \frac{2\pi}{c} j_1 R\{2A\zeta(1-\zeta)\theta(1-\zeta)\boldsymbol{e}_\theta + [(1-\zeta^2)\theta(1-\zeta) + \epsilon]\boldsymbol{e}_z\} ,$$

where an intergalactic magnetic field has been chosen which is longitudinal and is characterized by the free parameter ϵ, $|\epsilon| < 1$. Models which invert the direction of the longitudinal component of the magnetic field outside and near the border of the current region can be obtained by choosing negative ϵ values. The equilibrium will not be changed even if a longitudinal mass flow is present in the thermal structure.

On the cylindrical magnetic field structure we now superpose a conical distribution of relativistic electrons, the axis of the cylinder and the cone being coincident. As pointed out by many authors, the pitch angle distribution of the radiating electrons in extragalactic sources is unknown. In the general case the distribution function can be written in the following form:

$$F(E, \hat{\boldsymbol{v}}, \boldsymbol{r}) = N(E)n(\hat{\boldsymbol{v}})f(\boldsymbol{r}) , \tag{4.1}$$

where

$$\hat{\boldsymbol{v}} = \frac{\boldsymbol{v}}{|\boldsymbol{v}|} .$$

Let us introduce a coordinate system (x', y', x'), with the z'-axis parallel to the line of sight, the y'-axis along the projection of the axis on the plane of the sky, and with the origin on the cylinder axis, in such a way that the line of sight lies in (x', z')-plane as shown in Figure 1. If we suppose flux conservation for the relativistic electrons along the jet axis, their spatial distribution in the plane which contains the line of sight ($y' = 0$), at a given distance from the core, will be the following:

$$f(x', r, z'\delta, \beta) = \tan^{-2}\beta\left(z_0 + \frac{s\sqrt{r^2 - x'^2}}{\tan\delta}\right)^{-2}\theta(x', r, z') \tag{4.2}$$

where β is the opening angle of the conical relativistic electron distribution, z_0 is the distance from the vertex of the cone to the origin of the reference system (see Fig. 1), and r is the usual cylindrical coordinate which can be expressed as a function of x' and z' as $r = (x'^2 + z'^2 \sin^2\delta)^{1/2}$. The quantity δ is the angle between the line of sight and the jet axis (i.e., the angle between the z'-axis and the z-axis), defined to be positive when the jet is pointing in the half-space $y' > 0$. The functions θ and s are defined as follows:

Case (*a*): $z' \geq 0$, $|\delta| \leq 90°$, or $z' < 0$, $|\delta| > 90°$:

$$\theta(x', r, z') = 1, \quad s(x', r, z') = 1 \qquad \begin{cases}\text{if } |x'| < z_0 \tan\beta, |x'| < r < R^+; \\ \text{if } |x'| > z_0 \tan\beta, R^- < r < R^+;\end{cases}$$

$$\theta(r, z', x') = 0 \qquad \text{otherwise.}$$

Case (*b*): $z' < 0$, $|\delta| \leq 90°$, or $z' \geq 0$, $|\delta| > 90°$:

$$\theta(x', r, z') = 1, s(x', r, z') = -1 \qquad \text{if } |x'| < z_0 \tan\beta, |x'| < r < R^-;$$

$$\theta(r, z', x') = 0 \qquad \text{otherwise.}$$

The quantity $R^{\pm}$ represents the borders of the relativistic electron distributions along the line of sight; in this treatment we will not consider the case of relativistic electrons diffusing outside the current region ($R^{\pm} > R$). Explicit expressions of $R^{\pm}$ are given in Appendix B.

According to what has been studied in §§ II and III, we would like to take into account the streaming of electrons in only one direction along the field lines. The distribution function of the radiating electrons in the velocity space can then be represented by

$$n(\hat{v}) = \frac{1}{2}\left[1 + \tanh\left(\frac{\hat{v}\cdot\boldsymbol{B}}{wB}\right)\right]. \tag{4.3}$$

In this expression, which models in a simple way the fact that relativistic particles with $v_{\parallel} > 0$ are mostly present in the distribution function, w represents a measure of the steepness of $n(\hat{v})$ for $v_{\parallel} = 0$. For $w = 0$, we have a distribution of electrons which is uniform in the region $v_{\parallel} > 0$ and zero for $v_{\parallel} < 0$. For $w = \infty$, we recover the isotropic case. Because of the properties of synchrotron radiation, only particles with $\boldsymbol{v}$ oriented along the line of sight will be seen; we can then substitute in equation (4.3) the electron velocity vector with the vector of the line of sight.

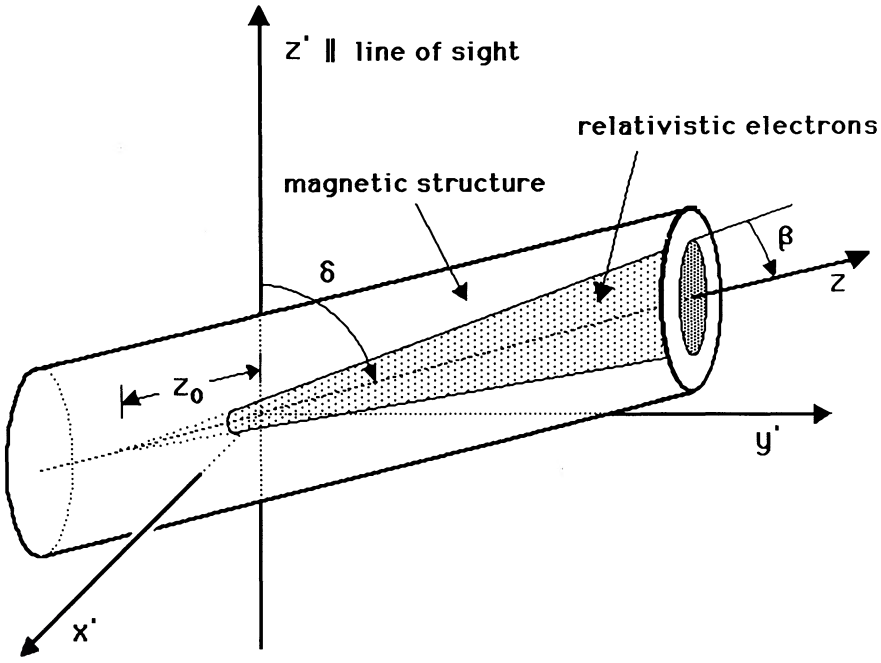

FIG. 1.—The cylindrical current region and the conical distribution of relativistic electrons representing a radio jet at an angle δ with the line of sight $\boldsymbol{K} \parallel z'$. In the particular reference system y' is the projection of the jet axis on the plane of the sky.

Finally, we take for the radiating electrons the usual energetic spectrum,

$$N(E)dE = N_0 E^{-(2\gamma+1)} dE ,$$

and assume that radiating regions are optically thin.

Now we can compute the Stokes parameters I, Q, and U along the line of sight for the given equilibrium configuration of the magnetic field and distribution of relativistic electrons. Nevertheless, for completeness purposes and to distinguish between effects due to the anisotropic term (eq. [4.3]) or to the spatial distribution of electrons and magnetic fields, we have shown results for both the isotropic and the anisotropic cases. Laing (1981) already gave the expressions for the Stokes parameters in some cases, as for a uniform helical field filling a cylinder or for a transverse self-similar CH field. It should be noticed that, for both these models, longitudinal variations are possible only if the pitch angle of the magnetic field or the inclination of the jet with respect to the line of sight varies along z. In our case instead, for given (A, ϵ) values, the spatial distribution of relativistic electrons is changing as we take different values of z_0; i.e., as we examine regions of the jet at different distances from the core (see Fig. 1). Since z_0 is the distance of our line of sight from the vertex of the cone, it represents in reality the parameter we should vary in studying longitudinal variations of the Stokes parameters. As z_0 increases, the relativistic electrons light up wider and wider regions of the magnetic field radial profile. Transverse profiles, from the jet axis to the outer borders, are instead obtained by varying the coordinate x'.

In Appendix B we give the analytical expressions for the spatial dependence of three Stokes parameters, I, Q, U, computed for an isotropic distribution of relativistic electrons ($w = \infty$) and for a convenient value of the spectral index ($\gamma = 1$). Numerical computations have shown that the variations of the Stokes parameters along the jet are negligible as we vary γ in a range of values compatible with observations. There are only small differences in the absolute values of the total intensity.

We should calculate the total intensity I, the degree of polarization $p = (Q^2 + U^2)^{1/2}/I$, and the structures of the apparent magnetic field configurations vary for different values of A, ϵ, δ, β, x', and z_0. But, first of all, we want to point out that the Stokes parameters do not depend strongly on the opening angle of the radio-emitting region as long as this stays below 10°, and this is usually the case for many of the observed radio jets. We can then use the widening of the relativistic electron distribution, $z_0 \tan \beta$ (varying between 0 and R, or 0 and 1 in units normalized to R) as a parameter which characterizes profiles taken at different distances from the vertex of the cone. For the anisotropic case we have chosen to show transverse profiles at two different distances from the vertex of the cone. In such a way it is easy to find out longitudinal variations as the electrons diffuse and light up different regions of the magnetic field.

Figures 2, 3, and 4 show the transverse intensity I/I_0 and degree of polarization $P = p/p_0$ for the cases $A = 1$, $A = 2$, $A = 4$, and with the following parameters (lengths are normalized to R):

$$\gamma = 0.6; \quad \delta = 30°, 60° 90°; \quad \epsilon = -0.3, 0.0, 0.3; \quad \begin{array}{ll} z_0 \tan \beta = 0.25, 0.95, & \text{for } w = 0.05; \\ z_0 \tan \beta = 0.95, & \text{for } w = \infty. \end{array}$$

Plotted curves are labeled according to whether B is mainly parallel or perpendicular. A sudden change in the sign of the derivative of p often indicates a transition from $B_{\parallel}$ to $B_{\perp}$. Sometimes the transition implies a nonnegligible region of the apparent magnetic field at intermediate angles. Examples of predicted polarization maps are given in Figure 5.

If both the magnetic field and the relativistic electron distribution have cylindrical symmetry and do not show systematic variations along z, it is well known, as Laing (1981) has already shown, that the apparent magnetic field is longitudinal or perpendicular to the jet axis, so there is no need to compute the Stokes parameter U which is identically zero. But in our case U can be different from zero in certain areas. The nontrivial magnetic structures (i.e., apparent field direction different from 0° or 90°) are effects due to the electron distribution which does not light up the far and near side of the jet symmetrically with respect to the line of sight when the jet is at an angle $\delta \neq 90°$. This effect should then be more visible for jets with wider opening angles or in regions far from core (where, in reality, departures of the apparent magnetic field direction from the parallel or orthogonal case are more commonly observed). Notice also that much larger areas where the apparent field is not parallel or orthogonal can be obtained for our model only when the relativistic electron region is decentered with respect to the current axis. When the jet is pointing away from us or is forming a negative angle with respect to the line of sight, the profiles shown in Figures 2, 3, 4, and 5 can invert their symmetry with respect to the axis of the magnetic structure. But this can be easily seen from the expressions of $B_{\perp}$, $\cos 2\chi$, and $\sin 2\chi$ given in Appendix B and from the expression of the distribution of the velocity of the electrons (eq. [4.3]).

The main effect of our anisotropic pitch angle distribution for the radiating particles is to make one side of the cylinder more luminous than the other when the predominant $\boldsymbol{B}$ component is the azimuthal one (especially when $\delta \approx 90°$). Jets which are at negative angles with the line of sight will be brighter on the opposite side with respect to the axis of the magnetic field structure. In both cases the visible region will not be centered on the axis of the magnetic field structure. When B is predominantly longitudinal, the effect of anisotropy will be instead to make the jet pointing toward us more luminous and the other jet less luminous. As we will see better in the next section, this will constitute a natural explanation to the one-sidedness phenomenon.

V. DISCUSSION

A model for extragalactic radio jets needs to be self-consistent from the theoretical point of view, but, most of all, it should predict observable quantities which agree with today's available data. The results of theoretical analysis on equilibrium, stability, and turbulence development for our magnetized jet model point out a distribution of relativistic particles which gives rise to a set of observable properties that we have derived in the previous sections. In this section we would like, first of all, to give a summary of the main features of the predicted observables, as the total and polarized intensity distribution, over a wide range of model parameters. In a second subsection we will then try to fit our model to the data of the most resolved radio jets. It is clear that effects such as depolarization by thermal matter or fast-growing instabilities can alter the observed quantities that we have just computed,

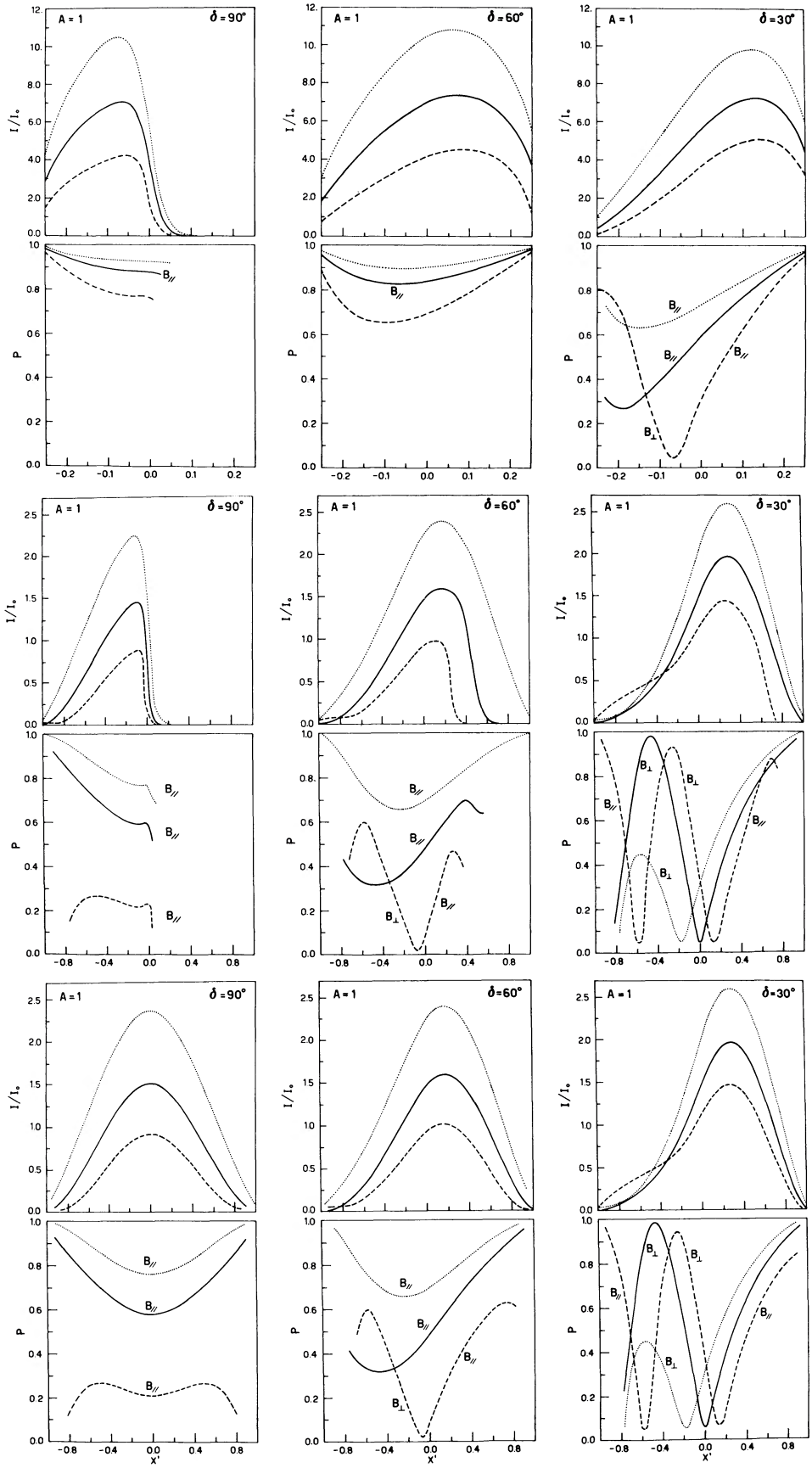

FIG. 2.—Transverse brightness, I/I_0, and polarization profiles, $P = p/p_0$, for $A = 1$ and different values of δ. They are plotted as a function of x' normalized to R. The three curves in each plot are for $\epsilon = 0.3$ (*dotted line*), $\epsilon = 0$ (*solid line*), and $\epsilon = -0.3$ (*dashed line*); The spectral index is $\gamma = 0.6$, the opening angle $\beta = 5°$. The three plots at the top are for region near the core, $z_0 \tan \beta = 0.25$, and $w = 0.05$. The three plots in the middle are for $z_0 \tan \beta = 0.95$ and $w = 0.05$, and the three at the bottom for $z_0 \tan \beta = 0.95$, and $w = \infty$ (isotropic case). The polarization curves are labeled according to the mean apparent magnetic field direction.

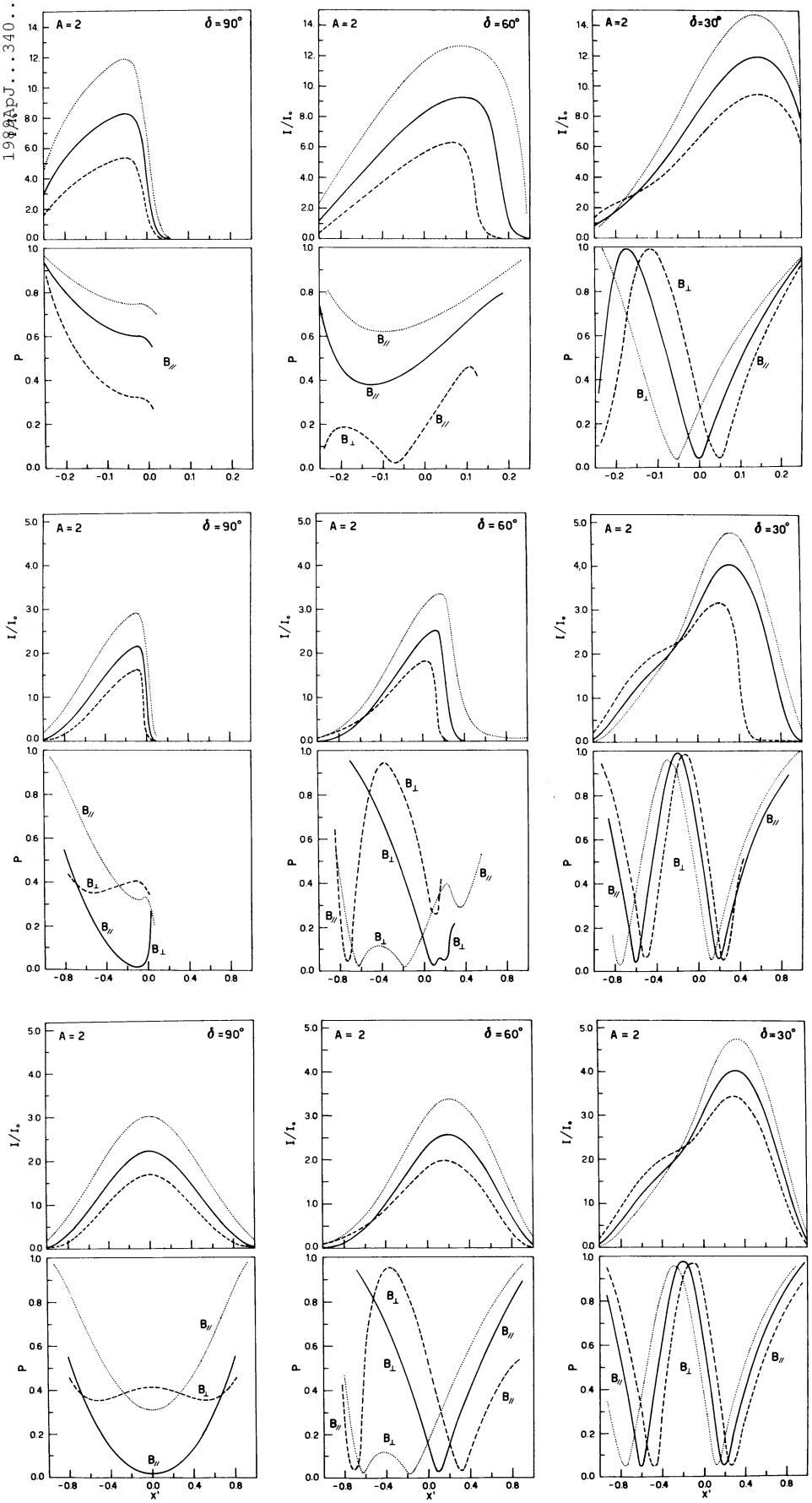

FIG. 3.—Transverse brightness, I/I_0, and polarization profiles, $P = p/p_0$, for $A = 2$ and different values of δ. Other parameters as in Fig. 2.

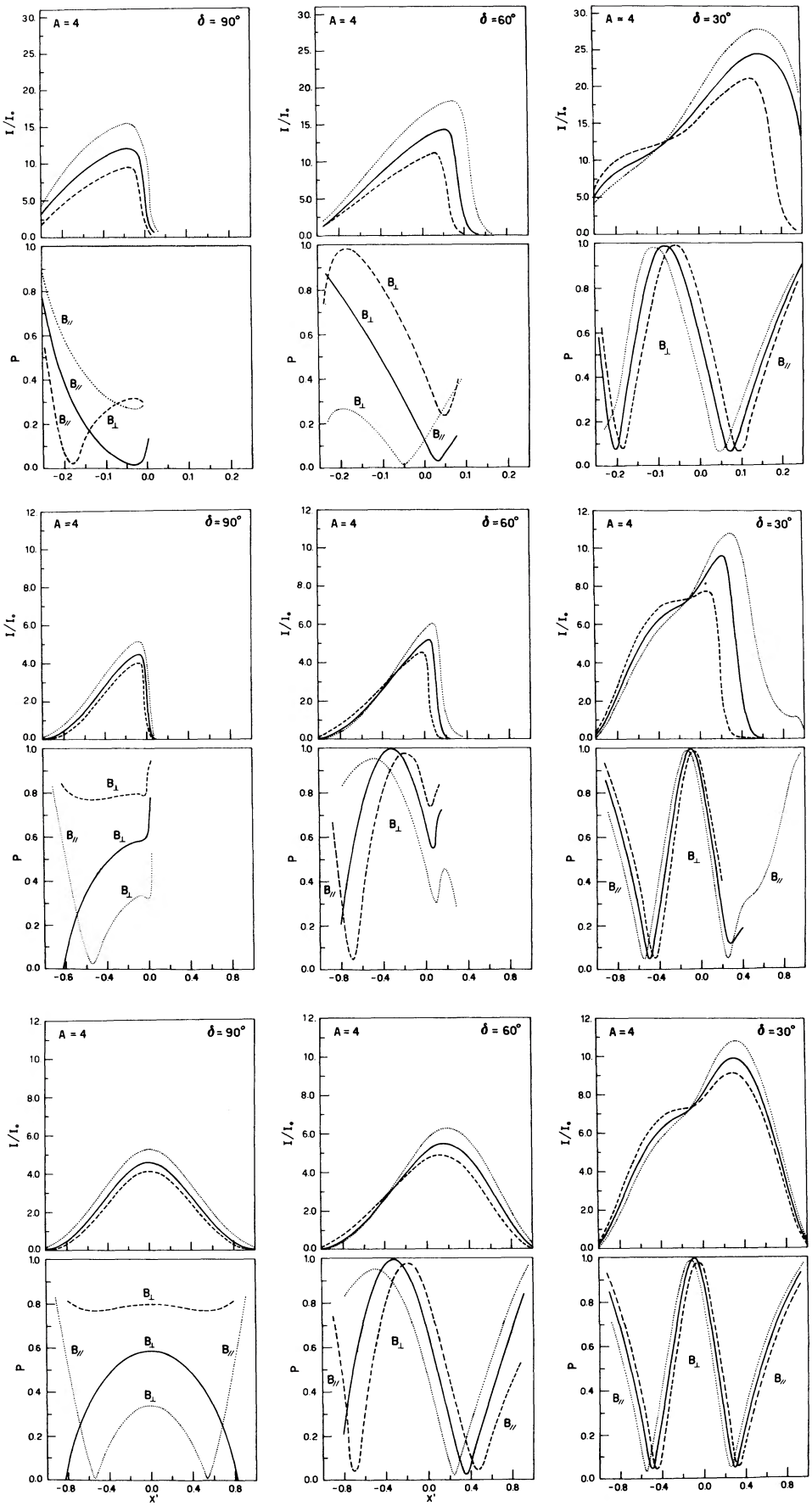

FIG. 4.—Transverse brightness, I/I_0 and polarization profiles, $P = p/p_0$, for $A = 4$ and different values of δ. Other parameters as in Fig. 2.

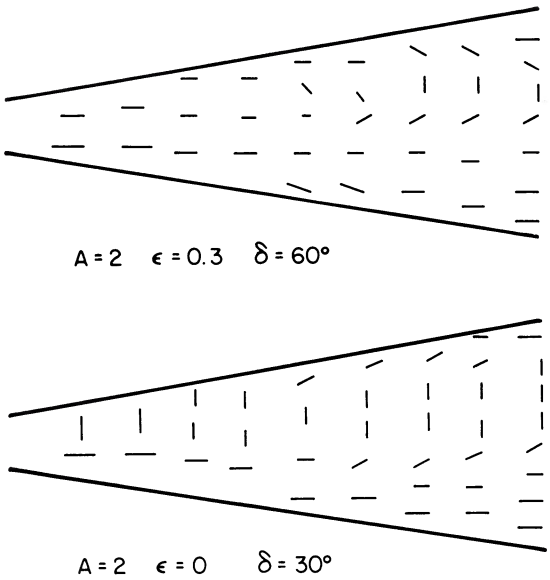

FIG. 5.—Some examples of apparent magnetic field variations along the radio jet for models with $A = 2$ and $w = 0.05$

they should be taken into account if we want a quantitative and more accurate fit of the data (small fluctuations of the magnetic field lines do not give appreciable depolarization). On the other hand, it is also true that variations of the equilibrium parameters, such as the addition of ordered motion for the thermal structure, could modify slightly the range of stable parameters, the instability growth rates, etc. For these reasons we will not put strict limits on the possible model parameters, but we will use the results of the analysis made in Paper I and in the previous sections to give qualitative estimates of the radio jet properties and to compare these with the observations.

a) Summary of Predicted Observable Quantities

i) *Longitudinal Variations of the Total and Polarized Intensity*

As we have already emphasized, the current region can be entirely uneven from the radio-emitting zone. Since the former region, together with the magnetic field, is expanding at a rate much lower than the opening angle of the observed jets (see § III), the magnetic field intensity is by no means proportional to $1/R^*$ or $1/R^{*2}$. Thus to explain the slow decrease of surface brightness (Bridle and Perley 1984), there is no longer a need for either a field amplification or a strong particle acceleration. The intensity along the jet will decrease mainly as a result of the diffusion of the relativistic electrons as they travel away from the source core, i.e., the average slope will be proportional to $1/R^*$. A more accurate fitting of the intensity peaks along the jet will depend on how the intensity is redistributed between the jet axis and its sides, which is a function of the model parameters (see Figs. 2, 3, and 4). Smaller corrections also need to be applied when relativistic particles die far from the core or eventually get reaccelerated.

The knots, which appear as spurious peaks in the longitudinal profiles of the total intensity and as shrinkage of the isophot contours, can be places where particles are not only reaccelerated but where the whole jet structure is changing geometry. What we mean by this is that knots can be places where a real shrinkage, like a bottleneck in the tri-dimensional jet structure or a bending of the jet relative to the line of sight, is taking place (Bicknell and Henriksen 1980; Königl and Chonduri 1985). These can be what is left of an $m = 0$ or $m = 1$ mode (Paper I) for instabilities which are still growing, or which, after saturation, might have originated a nonlinear cascade toward smaller wavelengths and eventually powered an acceleration mechanism. The $m = 1$ instability associated with an anisotropic distribution of relativistic electrons will make the part of the jet bending toward us more luminous, generating a peak in the longitudinal brightness profiles, and make the part pointing in the opposite direction less luminous. The distance between two knots is typically a few times the apparent diameter of the jet (NGC 6251; Perley *et al.* 1984), and we have seen (Paper I) that there are $m = 1$ modes at these wavelengths. The polarization does not have a simple expression even at the center of the jet ($x' = 0$) and in the isotropic case (Appendix B). However, comparing the radial profiles shown in Figures 2, 3, and 4 at different distances from the core, we can understand its longitudinal behavior. For fields which are predominantly longitudinal our prediction is that the level of polarization is high and almost uniform across the jet, unless the jet is oriented at small angles with the line of sight. This agrees with what is observed in the jets of the most powerful radio sources such as QSOs, where the apparent field is longitudinal and the polarization is high.

For magnetic field models with larger values of A, the apparent magnetic field is parallel near the core, the peak of fractional polarization decreases moving away from the nucleus until the jet starts displaying an apparent transverse magnetic field, and then it increases again. Oscillations in p different from these should be explained as bends in the jet structure. This is possible because the dependence of the maximum degree of polarization on δ is not monotonic (as it was for most of the models examined by Laing 1981).

ii) *Transverse Profiles of Total and Polarized Intensity*

Models with $A \leq 1$ and $\delta \approx 90°$ show distributions of total brightness, fractional polarization, and apparent field orientation which are symmetric with respect to the jet axis (Figs. 2, 3, 4), as it was for the helical and CH fields (Laing 1981). However, for other

parameters, bumps and marked asymmetries with respect to the jet axis can show up. Asymmetries due to a rapid decrease of the intensity on only one side of the jet axis (for $x' > 0$ or $x' < 0$, depending on δ) are mainly due to the anisotropic distribution of drift velocities of the radiating particles with respect to the field lines. These are especially visible when the jet is oriented perpendicularly to the line of sight. Where the field has a nonnegligible azimuthal component, the main effect of the anisotropy will be then to make one side of each jet less luminous (or invisible). One possibility for checking this effect would be to compare the slope of radial intensity profiles on both sides of the jets, because anisotropy will make the radial fall-off of the intensity steeper only on one side of the jet (Figs. 2, 3, 4). However, for most of the jets we have only isophot contours which do not give us detailed radial intensity profiles. We would like to have more resolved transverse profiles in order to prove this hypothesis unquestionably.

The bumps in the total brightness distribution, such as those shown in Figure 4 for $\delta = 30°$, 60°, also in the isotropic case, are intrinsic to the equilibrium model having a different spatial distribution for the magnetic structure and relativistic particles. Negative values for the parameter ϵ and low A values reduce the intensity quite a bit. Radially the polarization is more uniform at $\delta = 90°$ and for negative ϵ values. When the field is not longitudinal, one or both edges have a high degree of linear polarization.

iii) *The Apparent Magnetic Field Structure*

The apparent magnetic field $\boldsymbol{B}_a$ predicted by the models is always longitudinal near the core of the radio sources but becomes transverse further out. The transition is more rapid as A increases, or ϵ or δ decreases. We have plotted in Figure 6 at what distance from the core the apparent magnetic field starts to become transverse for three values of δ and for $\epsilon = 0$ (we have used $\beta = 5°$, but changes are small for $\beta < 10°$). The transition distance is given in units of $z_0 \tan \beta$ ($= 1$ when the relativistic particles have reached the outer border of the current region). Notice that this transition does not necessarily occur at the center of the current structure or at the brightness peak if $\delta \neq 90°$.

The quantity $\boldsymbol{B}_a$ can be different from being parallel or perpendicular when the jet is inclined at an angle $\delta \neq 90°$. This is because the far and near sides of the jet along the line of sight are not lighted up equally from the distribution of the relativistic electrons. Nevertheless, in order to have large areas of uniformly inclined apparent field, different from 0° or 90°, the distribution of relativistic electrons should be decentered with respect to the current region. We can have a semicircular structure in the apparent field (Fig. 5) as those observed near the end of the jet NGC 6251 and 3C 236. It is essential to point out that these structures, which show up for $\delta < 60°$, sometimes tend to be connected with asymmetries in the total radial intensity profiles, and this connection is noticeable in the data of the well-resolved structure of NGC 6251 jet (see § V*b*). It is unlikely that this correlation occurs in the case of the random magnetic field distribution studied by Laing (1981), where semicircular structures for $\boldsymbol{B}_a$ were also obtained.

As we can see from Figures 2, 3, and 4, there are also various cases where the field stays longitudinal only on one or both edges, depending upon A, ϵ, δ, w, and the distribution of the relativistic electron velocities along the field lines (the ϵ dependence for the apparent field structure, as well as for other observable properties, is less evident for high A or low δ values).

Finally, we would like to point out that when the magnetic field is predominantly longitudinal, anisotropy for the distribution of relativistic velocities is a natural explanation for the one-sidedness effect. As already pointed out in the introduction, we know that two-sided jets are less common when the apparent field is parallel to the jet axis. Many authors believe that the one-sidedness effect is due to the relativistic bulk motion of material at very small angles with the line of sight, but there is no compelling evidence for this motion on large scales. Also, to make the jet pointing toward us very luminous and the other one invisible, the direction of the jet kinetic motion needs to be at a very small angle with the line of sight, which is not statistically justifiable and also would not explain the observed correlation between one-sidedness and longitudinal apparent magnetic field.

Anisotropy in the distribution of the relativistic electrons will instead make the jet pointing away from us invisible, whenever $\boldsymbol{B}$ is more or less parallel to the jet axis and the inclination δ is in a range of angles between 90° and 270°. The exact width of the range of possible values of δ depends upon the values of A and the characteristics of the anisotropic distribution of electrons. The more luminous jet is pointing toward us, but not necessarily at small angles with our line of sight; the electrons, streaming along longitudinal field lines, will make the visible jet more collimated and more luminous than in other types of sources. Radio sources with nonnegligible azimuthal components of magnetic fields are weaker sources, and they have faster growth rates for unstable

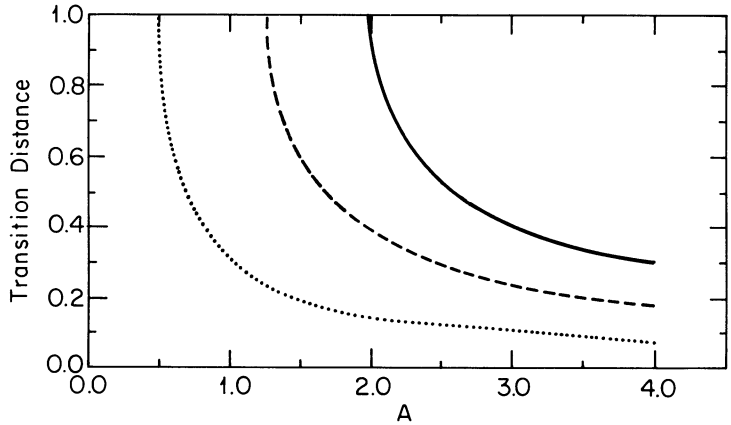

FIG. 6.—Distance from the region near the core, where electrons get injected, to the point where the apparent magnetic field starts to be transverse to the jet axis (at some x'). This is plotted as a function of the equilibrium parameter A for $\epsilon = 0$, $\delta = 90°$ (*solid line*), $\delta = 60°$ (*dashed line*), and $\delta = 30°$ (*dotted line*). It is given in units of $R/\tan \beta$. The β dependence being very weak, this plot is valid in the whole interval $0° < \beta < 10°$.

modes (Paper I). As we have seen in § II, being the magnetic field fluctuations proportional to the square root of $v\tau_A$ (eq. [2.1]), it is not surprising that these jets are also less collimated.

b) Model Fits to Properties of Observed Jets

In what follows we will try to choose among our models those which give a reasonable fitting to some of the best known radio jets. We will start examining the NGC 6251 jet whose structure is today the most resolved of all (Perley, Bridle, and Willis 1984). The characteristics of the NGC 6251 jet can be summarized as follows.

The structure is very collimated with an average opening angle $\approx 3°$, and there is a very faint counterjet, which is barely visible. In the bright jet there are three distinct regions, the first extending up to 100′ from the core with a decreasing average luminosity and a projected magnetic field which is dominated by the component parallel to the jet axis. A second region follows which is much less bright. Finally, at distances $>200'$, a third region can be seen where the luminosity increases significantly, and there is a clear misalignment or bend of the jet on the plane of the sky. Everywhere along the jet there are also sporadic brightness peaks. This is the only jet for which the transverse intensity profiles are known with enough accuracy, and they are more or less Gaussian in shape, very similar to what our model predictions are. For this jet some of our models work quite well in explaining the radial and longitudinal brightness profiles available, as well as the polarization and the apparent field structure. The field is parallel to the jet axis in regions near the core, as we expect from all of our models, and the polarization decreases due to an enlargement of the lighted region (after a few kiloparsecs from the core, where the field becomes well organized). The bright peak which follows this region at almost 30′ from the core is in a region where the apparent field is at intermediate angles, suggesting that the jet might have small bendings with respect to the line of sight (such as oscillations for an $m = 1$ mode) and the relativistic electron distribution gets decentered with respect to the jet axis. The comparison of the observed transverse intensity and polarization profile at 22′ with our profiles near the core in Figures 2, 3, and 4 shows an anisotropic distribution of relativistic particles near the core over a structure which, on average, is nearly perpendicular to the line of sight and has an MHD equilibrium model with $A = 2, \epsilon \geq 0$. On the jet side where the brightness profile is sharper, due to the anisotropy, the degree of polarization is lower and in agreement with what is shown in Figure 3 near the core. The profile at 32′ is just a wider region of the structure lightened up by the relativistic electrons. At 50′ the jet looks as if it starts bending away from us for a length much larger than the radio-emitting region radius. The intensity there is in fact decreasing, is more radially symmetric, and the apparent field becomes orthogonal in the central region. The radial behavior of the degree of polarization looks very similar to what is shown in Figure 3 for the anisotropic case, $\delta = 60°$ and $\epsilon \geq 0$.

At 127′ the jet still has a very low surface brightness, but soon after the brightness increases as if the jet pointed toward us to complete the oscillation. At 208′ and 227′ the intensity shows asymmetries typical of a jet which forms a small angle with the line of sight according to our model. Notice that the apparent magnetic field is parallel to the jet axis at the edge of the radio-emitting regions and shows semicircular structures in the farthest part. By comparing the total intensity profiles and the apparent field structure for $A \geq 2$ and $\delta \approx 30°$ we see again a very good agreement between the data and our model. This is also the case for the degree of polarization which has a maximum at the center and, as the profile at 227′ shows clearly, rises again near the edges, where the apparent field is parallel. Nevertheless, changes in ϵ, negative values for example, are required if A is constantly ≈ 2 along the jet. The inversion of symmetry in the intensity profile shape between 208′ and 227′ could be again explained in terms of small-wavelength oscillations of the jet which points toward and away from us.

Values of A slightly greater than 2 seem instead to be required for modeling the two jets of 3C 31 (Fomalont *et al.* 1980). The data show that both jets have a low opening angle: the less luminous has the apparent magnetic field orthogonal over the whole jet, while the other has a clear transition of the apparent field from parallel to perpendicular at distance $d = 2R$, where R is of the order of the radius of the radio-emitting region in the farthest point. The apparent magnetic field shows the shape of a half-circumference near the end. For the brightest jet the polarization and luminosity increase near the core, where relativistic particles are generated. Further away the luminosity stays constant, while the polarization slowly increases, the field becomes orthogonal, and p gets centrally peaked. The model can again explain the transition of the apparent field with no need for field amplification, but in order to fit the field transition at a small distance from the core, the jet should be inclined with respect to the line of sight, and large values of A are required (see Fig. 6). Models with a high value of A and models where the farthest part of the jet is strongly inclined with respect to the line of sight are both able to give the typical circular structure of the apparent field and a rapid transition from parallel to perpendicular. The polarization increases going from the core of the source to the radio lobes (while the luminosity stays constant), it is higher at the edges near the core but has centrally peaked profiles in the more distant regions. If we want to reproduce this polarization behavior, without taking into account possible additional effects, we must choose high values of A. Similar values of A and δ would be required to explain the structure of the less luminous jet. Notice also the curvature of the intensity contours on the plane of the sky for this jet. This reminds us that such models have MHD structures with stability problems and modifications of the MHD equilibrium model, as well as a more detailed analysis of the saturation and evolution of the instabilities is needed.

In the bright jet of NGC 315 (Willis *et al.* 1981) the asymmetries in the polarization distribution and intensity contours with respect to the jet axis are very indicative of an anisotropic distribution of relativistic electrons with respect to the field lines of the type examined in the previous sections. Looking at models with intermediate values of A ($1 < A < 2$) and $\delta < 60°$, we can see in fact that anisotropy can generate an apparent magnetic field which is predominantly parallel only on one edge, where the intensity goes down more smoothly, as it is for the NGC 315 jet. Anisotropy could also help in keeping low the degree of polarization observed in the farthest part of the jet, as well as in justifying the absence of a visible counterjet. But since models with $1 < A < 2$ have a magnetic field with a nonnegligible azimuthal component, it is not clear whether the directive properties of synchrotron radiation of streaming particles, plus a decrease in the intensity due to the relativistic motion of electrons, are sufficient to explain the one-sidedness of jets such as NGC 315.

This argument looks instead more convincing for explaining the one-sidedness of the most luminous sources, as we have already mentioned in the previous sections. In these sources the field is mainly longitudinal, and the high polarization and collimation of

these jets support the idea of a distribution of relativistic electrons at very narrow pitch angles around the magnetic field lines of a model with $A < 1$. The electrons move faster away from the nucleus, and the level of magnetic fluctuations is low, in agreement with the small growth rates of MHD instabilities for these models. To this class belong almost all the jets from quasar (e.g., 4CT 74.17.1; van Breugel and Willis 1981). These jets show $\boldsymbol{B}_a$ always parallel to the axis except in some cases near the very end of the structure (1857+566; Saikia *et al.* 1983). As the models predict, the polarization is higher near the edges. Where one of the knots of the 4CT 74.17.1 jet occurs, the rapid radial decrease of the intensity and the higher degree of linear polarization support the idea of the anisotropic distribution of electrons, described previously, and the bending of the jet where the knots appear. The $A < 1$ models can be applied to some two-sided jets. This is, for example, the case for 3C 465 (van Breugel 1980), where the apparent magnetic field is longitudinal.

There is still another group of jets which have the apparent magnetic field always orthogonal to the jet axis. In NGC 5127, for example (Fanti *et al.* 1982), the two jets look completely symmetric, and the polarization increases going toward the lobes and is centrally peaked. A high value of A can easily reproduce these structures, but the theory of turbulence derived in § II applies only if there is a modification of the equilibrium model or other additional effects able to keep the level of magnetic field fluctuations low. If this is the case, the anisotropy in the relativistic electron distribution over an almost azimuthal magnetic field can make one side of the jet, pointing at $\delta < 180°$, more luminous as well as the opposite side for the jet pointing in the other direction (and the two jets will always look symmetric with respect to the central galaxy). The axis of the current region and that of the relativistic electron distribution are then predicted to be not at the center of the radio-emitting region but shifted with respect to one side of the emission. A behavior of the apparent field and polarization similar to NGC 5127 is shown in the weak radio structures examined by Morganti *et al.* (1987). Nevertheless, we have to admit that the very common circular structures of the apparent magnetic field at the end of both jets are more likely due to a real distortion of the field lines encountering the external medium, which we know to be substantial for these class of radio sources, or to other physical phenomena in the jets (see Morganti *et al.* 1987 for details).

Finally, we would like to point out in Figures 2, 3, and 4 models which predict the apparent magnetic field to be longitudinal only at the edges, as is observed in jets such as NGC 1399 (Killeen, Bicknell, and Ekers 1987) and 3C 66B (van Breugel 1982).

Our conclusion is that interesting results emerge from modeling the structure of the radio jets by decoupling the structured magnetic field region from the radio-emitting area. In particular, we have considered a cylindrical thermal structure obeying the MHD model analyzed in Paper I and a distribution of relativistic particles which diffuse out from the core following the magnetic field lines. The spatial diffusion turns out to be efficient because of turbulent fluctuations at small wavelengths where the energy has been carried out by the nonlinear interaction between instability modes. The low widening of the radio-emitting region and an anisotropic distribution of radiating particles are then natural consequences of this diffusion and give an interesting explanation to the one-sidedness phenomena of the most powerful radio sources. The even lower expansion of the thermal structure rules out the hypothesis that the magnetic field intensity is proportional to $1/R$ and predicts a decrease of the brightness more similar to what has been observed.

Remarkable are also other fits to the observations, such as those concerning the radial intensity profiles of NGC 6251, the polarization and the transition of the apparent magnetic field from parallel to perpendicular to the axis of many jets, etc. This encourages further developments of these types of models, as well as new and more resolved observations of radio jets.

APPENDIX A

In this Appendix we will set up an explicit expression for the autocorrelation tensor of the fluctuating magnetic field. As usual, we shall work in Fourier space and introduce the decomposition of $\delta\boldsymbol{B}(\boldsymbol{r}, t)$ in spatial harmonics:

$$\delta\boldsymbol{B}(\boldsymbol{r}, t) = \Sigma_{\boldsymbol{k}}\, \boldsymbol{b}(\boldsymbol{k}, t) e^{i\boldsymbol{k}\cdot\boldsymbol{r}} ,$$

where $\boldsymbol{k} = (2\pi/L)(n_1, n_2, n_3)$, the n_i are positive or negative integers, the fields are assumed to be spatially periodic with period L, and the limit $L \to \infty$ is implied.

Since the magnetic field is divergenceless, we have

$$\boldsymbol{k} \cdot \boldsymbol{b}(\boldsymbol{k}, t) = 0 ,$$

so that the Fourier amplitude can be written as

$$\boldsymbol{b}(\boldsymbol{k}, t) = \sum_{\alpha=1}^{2} b_\alpha(\boldsymbol{k}, t) \boldsymbol{e}^{(\alpha)}(\boldsymbol{k}) , \tag{A1}$$

$\boldsymbol{e}^{(1)}(\boldsymbol{k})$ and $\boldsymbol{e}^{(2)}(\boldsymbol{k})$ being two arbitrary unit vectors which are mutually orthogonal and orthogonal to the wave vector $\boldsymbol{k}$. In the presence of a background magnetic field $\boldsymbol{B}_0$, the most natural choice is to take these unit vectors as

$$\boldsymbol{e}^{(1)}(\boldsymbol{k}) = \frac{i\boldsymbol{k} \times \boldsymbol{B}_0}{|\boldsymbol{k} \times \boldsymbol{B}_0|} , \qquad \boldsymbol{e}^{(2)}(\boldsymbol{k}) = \frac{i\boldsymbol{k}}{k} \times \boldsymbol{e}^{(1)}(\boldsymbol{k}) . \tag{A2}$$

Assuming statistical homogeneity, using expression (A1) and recalling that in the limit $L \to \infty$

$$\sum_{\boldsymbol{k}} \equiv (L/2\pi)^3 \int d^3\boldsymbol{k} ,$$

the autocorrelation for fluctuating magnetic field is easily found to be given by

$$\langle \delta B_i(\boldsymbol{r}, t)\delta B_j(\boldsymbol{r}, t)\rangle = \sum_\alpha \sum_\beta \int d^3\boldsymbol{k} U_{\alpha\beta}(\boldsymbol{k}, t) e_i^{(\alpha)} e_j^{(\beta^*)} , \tag{A3}$$

with

$$U_{\alpha\beta}(\boldsymbol{k}, t) = (L/2\pi)^3 \langle \boldsymbol{b}_\alpha(\boldsymbol{k}, t)\boldsymbol{b}_\beta(\boldsymbol{k}, t)\rangle .$$

By explicitly calculating $e_i^{(\alpha)} e_j^{(\beta^*)}$ in a reference frame with the z-axis parallel to $\boldsymbol{B}_0$, and assuming that the turbulence is statistically cylindrically symmetric around $\boldsymbol{B}_0$ it can be shown that the autocorrelation tensor reduces to

$$\langle \delta B_i(\boldsymbol{r}, t)\delta B_j(\boldsymbol{r}, t)\rangle = 2\pi \int_{-\infty}^{\infty} dk_\parallel \int_0^\infty k_\perp \, dk_\perp [\tfrac{1}{2}\delta_{ij} U_{11}(k_\perp, k_\parallel, t) + T_{ij} U(k_\perp, k_\parallel, t)] ,$$

with T_{ij} given by

$$\begin{pmatrix} k_\parallel^2/(2k^2) & 0 & 0 \\ 0 & k_\parallel^2/(2k^2) & 0 \\ 0 & 0 & k_\perp^2/k^2 \end{pmatrix} .$$

If we now introduce the quantities $U_\parallel(k_\perp, k_\parallel, t)$ and $U_\perp(k_\perp, k_\parallel, t)$ defined through

$$U_\perp(k_\perp, k_\parallel, t) = \left[U_{11}(k_\perp, k_\parallel, t) + \left(\frac{k_\parallel}{k}\right)^2 U_{22}(k_\perp, k_\parallel, t) \right] , \tag{A4a}$$

and

$$U_\parallel(k_\perp, k_\parallel, t) = \left(\frac{k_\perp}{k}\right)^2 U_{22}(k_\perp, k_\parallel, t) , \tag{A4b}$$

the expression quoted in equation (2.4) is finally recast.

It is, however, worth noting that calculations by Carbone and Veltri (1988) show that MHD turbulence, in presence of an average magnetic field due to nonlinear wave interactions, relax toward a state where

$$U_{11}(k_\perp, k_\parallel, t) \approx U_{22}(k_\perp, k_\parallel, t) \approx U(k_\perp, k_\parallel, t) ,$$

the only effect of anisotropy being given by the fact that $U(k_\perp, k_\parallel, t)$ depends in different ways from the arguments $k_\perp$, $k_\parallel$; the autocorrelation tensor of the magnetic field fluctuations can then be expressed in terms of $U(k_\perp, k_\parallel, t)$ only.

APPENDIX B

For a magnetic field and an isotropic distribution of relativistic electrons as described in this paper we compute the integrals of the total and polarized intensity for a jet which is inclined of an angle δ with respect to the line of sight. We give only the analytic solutions for spectral index $\gamma = 1$, but numerical evaluations (Figs. 2, 3, 4) have shown no significant dependence of the integrals on γ. In the reference system (x', y', z') described in § IV, the Stokes parameters along the line of sight are integrals of elliptical type and can be expressed as function of x' (projected radial distance from the jet axis), δ, and β (average opening angle of the relativistic electron distribution) for a given z_0 (distance of the origin of the reference system from the vertex of the cone). We will normalize all the lengths to the radius R of the current region.

The relativistic electron distribution, inside the jet (see eq. [4.1]), for the isotropic case ($w = \infty$) can be written as

$$F(E, \boldsymbol{r}) = N(E) f(x', r, z', \delta, \beta) = \frac{N(E)}{\tan^2 \beta} \left[\frac{r^2/\tan^2 \delta + n_2 + n_3 \sqrt{r^2/\tan^2 \delta - x'^2/\tan^2 \delta}}{(r^2/\tan^2 \delta + n_1)^2} \right] \theta(x', r, z') ,$$

with

$$n_1 = -x'^2/\tan^2 \delta - z_0^2 ,$$
$$n_2 = -x'^2/\tan^2 \delta + z_0^2 ,$$
$$n_3 = -2s(x', r, z')z_0 ,$$

and $s(x', r, z')$ and $\theta(x', r, z')$ are constants defined in § IV. Given the component of the magnetic field orthogonal to the line of sight, $B_\perp$, as

$$B_\perp = B\sqrt{1 - \left(\frac{x'}{r} \sin\eta \sin\delta - \cos\eta \cos\delta\right)^2} = = B\sqrt{b_4 r^4 + b_3 r^3 + b_2 r^2 + b_1 r + b_0} , \tag{B1}$$

where η is the pitch angle of the tri-dimensional helicoidal magnetic field measured from its axis, and

$$b_4 = 4A^2 + \sin^2\delta\,, \qquad b_3 = 4Ax'\sin\delta\cos\delta - 8A^2, \qquad b_2 = 4A^2(1 - x'^2\sin^2\delta) - 4Ax'\sin\delta\cos\delta - 2(1+\epsilon)\sin^2\delta\,,$$
$$b_1 = 8A^2x'^2\sin^2\delta - 4Ax'(1+\epsilon)\sin\delta\cos\delta\,, \qquad b_0 = \sin^2\delta[(1+\epsilon)^2 - 4A^2x'^2] + 4Ax'(1+\epsilon)\sin\delta\cos\delta\,,$$

we can express the Stokes parameters I, Q, and U along the line of sight at projected x' distance from the jet axis. After integrating on E, and for $\gamma = 1$, we can write

$$I = \frac{I_0}{\sin\delta}\int \frac{f(x', r, z_0, \delta, \beta)B_\perp^2}{\sqrt{r^2 - x'^2}}\,r\,dr\,, \qquad Q = \frac{Q_0}{\sin\delta}\int \frac{f(x', r, z_0, \delta, \beta)B_\perp^2}{\sqrt{r^2 - x'^2}}\cos r2\chi\,dr\,, \qquad U = \frac{U_0}{\sin\delta}\int \frac{f(x', r, z_0, \delta, \beta)B_\perp^2}{\sqrt{r^2 - x'^2}}\sin r2\chi\,dr\,, \tag{B2}$$

where χ is the position angle of the observed $\boldsymbol{E}$-vector on the sky measured counterclockwise with respect to y', and

$$\cos 2\chi = \frac{B_\theta^2(1 - x'^2/r^2) - (B_\theta\cos\delta\,x'/r + B_z\sin\delta)^2}{B_\theta^2(1 - x'^2/r^2) + (B_\theta\cos\delta\,x'/r + B_z\sin\delta)^2}\,, \qquad \sin 2\chi = \pm\frac{B_\theta\sqrt{1 - x'^2/r^2}(B_\theta\cos\delta\,x'/r + B_z\sin\delta)}{B_\theta^2(1 - x'^2/r^2) + (B_\theta\cos\delta\,x'/r + B_z\sin\delta)^2}$$

(the plus and minus sign refer, respectively, to the radiation from the far and near sides of the helix). The integration should be performed over the following intervals:

i) $|x'| \le r \le R^+$ and $|x'| \le r \le R^-$, when $|x'| < z_0\tan\beta$;
ii) $R^- \le r \le R^+$, otherwise;

with $R^\pm$ given by

$$R^\pm = \left\{x'^2 + \sin^2\delta\left[\frac{-z_0\cos\delta\tan^2\beta \mp \sqrt{\sin^2\delta\tan^2\beta(z_0^2 - x'^2/\tan^2\beta) + x'^2\cos^2\delta\tan^2\beta}}{\cos^2\delta\tan^2\beta - \sin^2\delta}\right]^2\right\}^{1/2}.$$

Solutions of the three indefinite integrals, $\tilde{I}$, $\tilde{Q}$, $\tilde{U}$, in equation (B2) can be expressed as follows:

$$\tilde{I} = \frac{1}{\tan^2\beta}\left[\frac{b_4}{3}(r^2 - x'^2)^{3/2} + \left(\frac{b_3 r}{2} + x'^2 b_4 + b_4 n_2 - 2n_1 b_4 + b_2\right)\sqrt{r^2 - x'^2} + \left(\frac{b_3 x'^2}{2} + b_3 n_2 - 2n_1 b_3 + b_1\right)\ln|r + \sqrt{r^2 - x'^2}|\right.$$
$$+ \frac{n_3}{4\sqrt{-n_1}}(3b_3 n_1 - b_1)\ln\left|\frac{\sqrt{-n_1} + r}{\sqrt{-n_1} - r}\right| + n_3\left(\frac{b_4 r^4}{2} - b_4 n_1^2 + b_3 r^3 + \frac{3n_1 b_3 r}{2} + \frac{b_2 n_1}{2} - \frac{b_1 r}{2} - \frac{b_0}{2}\right)\frac{1}{r^2 + n_1}$$
$$\left. + n_3\left(\frac{b_2}{2} - b_4 n_1\right)\ln|r^2 + n_1| + (A_1 + B_1)I_1 + (A_1 - B_1)I_2 + (C_1 + D_1)I_3 + (C_1 - D_1)I_4\right],$$

where

$$I_1 = -\frac{1}{\sqrt{(p^2 - x'^2)}}\ln|2\sqrt{(p^2 - x'^2)[(p^2 - x'^2)t^2 - 2pt + 1]} + 2(p^2 - x'^2)t - 2p|\,,$$

with

$$p = -\sqrt{-n_1}\,, \qquad t = \frac{1}{p + r}\,, \qquad \text{if} \quad r \ge \sqrt{-n_1}\,,$$
$$t = \frac{1}{p - r}\,, \qquad \text{if} \quad r < \sqrt{-n_1}\,.$$

$$I_2 = I_1\,, \quad \text{with} \quad p = \sqrt{-n_1}\,, \qquad t = \frac{1}{p + r}\,;$$

$$I_3 = \frac{\sqrt{(p^2 - x'^2)t^2 - 2pt + 1}}{p^2 - x'^2} + \frac{p}{p^2 - x'^2}I_1\,, \qquad p, t \text{ as for } I_1\,;$$

$$I_4 = -\frac{\sqrt{(p^2 - x'^2)t^2 - 2pt + 1}}{p^2 - x'^2} + \frac{p}{p^2 - x'^2}I_2\,, \qquad p, t \text{ as for } I_2\,;$$

$$A_1 = \frac{3n_1^2 b_4 - 2n_1(b_2 + b_4 n_2) + b_2 n_2 + b_0}{2}\,, \qquad B_1 = \frac{1}{4\sqrt{-n_1}}[b_1 n_2 + 5b_3 n_1^2 - 3n_1(b_3 n_2 + b_1)]\,,$$

$$C_1 = \frac{1}{4}[b_1 n_2 + b_3 n_1^2 - n_1(b_3 n_2 + b_1)]\,, \qquad D_1 = \frac{-1}{4\sqrt{-n_1}}[n_1^3 b_4 - n_1^2(b_2 + b_4 n_2) + n_1(b_0 + b_2 n_2)]\,.$$

It is clear that $\tilde{Q}$ has the same expression as $\tilde{I}$ if we substitute the constants b_i with c_i given by

$$c_4 = 4A^2 - \sin^2\delta\,, \qquad c_3 = -8A^2 - 4Ax'\cos\delta\sin\delta\,,$$
$$c_2 = -4A^2x'^2(1+\cos^2\delta) + 4A^2 + 2(1+\epsilon)\sin^2\delta + 4Ax'\cos\delta\sin\delta\,,$$
$$c_1 = 8A^2x'^2(1+\cos^2\delta) + 4Ax'(1+\epsilon)\cos\delta\sin\delta\,,$$
$$c_0 = -4Ax'(1+\epsilon)\cos\delta\sin\delta - 4A^2x'^2(1+\cos^2\delta) - (1+\epsilon)^2\sin^2\delta\,.$$

We have the following expression for $\tilde{U}$:

$$\tilde{U} = \frac{s}{\tan^2\beta}\left\{\frac{1}{r^2+n_1}\left[\frac{g_3}{3}r^5 + \frac{g_2}{2}r^4 + r^3\left(g_3n_2 - \frac{5}{3}n_1g_3 + g_1\right) + r\left(-\frac{5}{2}g_3n_1^2 + \frac{3}{2}n_1g_3n_2 + \frac{3}{2}n_1g_1 - \frac{g_1n_2}{2}\right)\right.\right.$$
$$\left. - g_2n_1^2 + \frac{g_2}{2}n_1n_2 + \frac{n_1g_0}{2} - \frac{n_2g_0}{2}\right] + \left[-5g_3n_1^2 + 3n_1(g_3n_2+g_1) - g_1n_2\right]\frac{1}{4\sqrt{-n_1}}\ln\left|\frac{\sqrt{-n_1}+r}{\sqrt{-n_1}-r}\right|$$
$$+\left(-n_1g_2 + \frac{n_2g_2}{2} + \frac{g_0}{2}\right)\ln|r^2+n_1| + \left[-n_3g_3\frac{x'^2}{2} + n_3(g_1 - 2n_1g_3)\right]\ln|r+\sqrt{r^2-x'^2}| + n_3\left(\frac{rg_3}{2} + g_2\right)\sqrt{r^2-x'^2}$$
$$\left. + (A_2+B_2)I_1 + (A_2-B_2)I_2 + (C_2+D_2)I_3 + (C_2-D_2)I_4\right\}\,,$$

where

$$g_3 = 2A\sin\delta\,, \qquad g_2 = 4A^2x'\cos\delta - 2A\sin\delta\,, \qquad g_1 = -8A^2x'\cos\delta - 2A(1+\epsilon)\sin\delta\,,$$
$$g_0 = 4A^2x'\cos\delta + 2A\sin\delta(1+\epsilon)\,,$$

$$A_2 = \frac{n_3}{2}(g_0 - x'^2g_2 - 2n_1g_2)\,, \qquad B_2 = \frac{n_3}{4\sqrt{-n_1}}(5n_1^2g_3 - 3n_1g_1 + 3n_1g_3x'^2 - x'^2g_1)\,,$$

$$C_2 = \frac{n_3}{4}(n_1^2g_3 - n_1g_1 + n_1g_3x'^2 - g_1x'^2)\,, \qquad D_2 = \frac{n_3}{4\sqrt{-n_1}}(n_1^2g_2 - g_0n_1 + x'^2n_1g_2 - x'^2g_0)\,.$$

For $\delta = 90$, $\tilde{I}$, $\tilde{Q}$, $\tilde{U}$ will have the simpler expressions:

$$\tilde{I} = \frac{1}{\tan^2\beta\, z_0}\left[\left\{\frac{r^3}{4}(4A^2+1) + \frac{r}{2}\left[-A^2x'^2 + \frac{3x'^2}{4} + 4A^2 - 2(1+\epsilon)\right]\right\}\sqrt{r^2-x'^2}\right.$$
$$\left. + \left[-\frac{1}{2}A^2x'^4 + \frac{3}{8}x'^4 - 2A^2x'^2 - x'^2(1+\epsilon) + (1+\epsilon)^2\right]\ln|r+\sqrt{r^2-x'^2}| - \frac{8}{3}A^2(r^2-x'^2)^{3/2}\right]\,,$$
$$\tilde{Q} = \frac{1}{\tan^2\beta\, z_0^2}\left[\left\{\frac{r^3}{4}(4A^2-1) + \frac{r}{2}\left[-A^2x'^2 - \frac{3x'^2}{4} + 4A^2 + 2(1+\epsilon)\right]\right\}\sqrt{r^2-x'^2}\right.$$
$$\left. + \left[-\frac{A^2x'^4}{2} - \frac{3}{8}x'^4 - 2A^2x'^2 + x'^2(1+\epsilon) - (1+\epsilon)^2\right]\ln|r+\sqrt{r^2-x'^2}| - \frac{8}{3}A^2(r^2-x'^2)^{3/2}\right]$$
$$\tilde{U} = \frac{sAr^2}{\tan^2\beta\, z_0^2}\left[\frac{2}{5}r^3 - \frac{1}{2}r^2 - \frac{2}{3}(1+\epsilon)r + (1+\epsilon)\right]\,.$$

REFERENCES

Barnes, A. 1978, in *Solar System Plasma Physics*, Vol. **11**, ed. C. F. Kennel, L. J. Lanzerotti, and E. N. Parker (Amsterdam: North Holland), p. 177.
Begelman, M. C., Blandford, R. D., and Rees, M. J. 1984, *Rev. Mod. Phys.*, **56**, 255.
Belcher, J. W., and Davis, L. 1971, *J. Geophys. Res.*, **76**, 3534.
Bendford, G., Ferrari, A., and Trussoni, E. 1980, *Ap. J.*, **241**, 98.
Bicknell, G. V., and Henriksen, R. N. 1980, *Ap. Letters*, **21**, 29.
Blandford, R. D., and Rees, M. J. 1974, *M.N.R.A.S.*, **169**, 395.
Bridle, A. H., and Perley, R. A. 1984, *Ann. Rev. Astr. Ap.*, **22**, 319.
Carbone, V., Einaudi, G., and Veltri, P. 1987, *Solar Phys.*, **111**, 31.
Carbone, V., and Veltri, P. 1987, *Astr. Ap.*, **188**, 239.
———. 1988, *J. Fluid Mech.*, submitted.
Chan, K. L., and Henriksen, R. N. 1980, *Ap. J.*, **241**, 534.
Chiuderi, C., Pietrini, P., and Torricelli-Ciamponi, G. 1989, *Ap. J.*, **338**, in press.
Coleman, P. J. 1968, *Ap. J.*, **153**, 371.
De Young, D. S. 1980, *Ap. J.*, **241**, 81.
———. 1982, in *IAU Symposium 97, Extragalactic Radio Sources*, ed. D. S. Heeschen and C. M. Wade (Dordrecht: Reidel), p. 69.
Dobrowolny, M., Mangeney, A., and Veltri, P. 1981, *Phys. Rev. Letters*, **45**, 144.
Eilak, J. 1979, *Ap. J.*, **230**, 373.
Fanti, R. 1983, in *Astrophysical Jets*, ed. A Ferrari and A. G. Pacholczyk (Dordrecht: Reidel), p. 253.
Fanti, R., Lari, C., Parma, P., Bridle, A. H., Ekers, R. D. and Fomalont, E. B. 1982, *Astr. Ap.*, **110**, 169.
Fomalont, E. 1983, in *Astrophysical Jets*, ed. A. Ferrari and A. G. Pacholczyk (Dordrecht: Reidel), p. 37.
Fomalont, E., Bridle, A. H., Willis, A. G., and Perley, R. A. 1980, *Ap. J.*, **237**, 418.
Ginzburg, V. L., and Syrovatskii, S. I. 1965, *Ann. Rev. Astr. Ap.*, **3**, 297.
Grappin, R., Frish, U., Leorat, J., and Pouquet, A. 1982, *Astr. Ap.*, **105**, 6.

Henriksen, R. N., Bridle, A. H., and Chan, K. L. 1982, *Ap. J.*, **289**, 173.
Jokipii, J. R. 1966, *Ap. J.*, **146**, 480.
Killeen, N. E. B., Bicknell, G. V., and Ekers, R. D. 1988, *Ap. J.*, **325**, 180.
Königl, A., and Choudhuri, A. R. 1985, *Ap. J.*, **289**, 173.
Lacombe, C. 1977, *Astr. Ap.*, **54**, 1.
Laing, R. A. 1980, *M.N.R.A.S.*, **193**, 427.
———. 1981, *Ap. J.*, **248**, 87.
Livshits, M. A., and Tsytovich, V. N. 1970, *Nucl. Fusion*, **10**, 241.
Matthaeus, W., and Montgomery, D. C. 1984, in *Statistical Physics and Chaos in Fusion Plasmas*, ed. C. W. Horton and L. E. Reichl (New York: Wiley), p. 285.
Melrose, D. B. 1968, *Ap. Space Sci.*, **2**, 171.
———. 1980, *Plasma Astrophysics* (New York: Gordon & Breach).
Morganti, R., Fanti, C., Fanti, R., Parma, P., and de Ruiter, H. R. 1987, *Astr. Ap.*, **183**, 203.
Owen, F. N., Hardee, P. E., and Bignell, R. C. 1987 *Ap. J. (Letters)*, **239**, L11.
Pacholczyk, A. G. 1970, *Radio Astrophysics* (San Francisco: Freeman).
Perley, R. A., Bridle, A. H., and Willis, A. G. 1984, *Ap. J. Suppl.*, **54**, 291.
Perley, R. A., Bridle, A. H., Willis, A. G., and Fomalont, E. B. 1980, *A.J.*, **85**, 500.
Perley, R. A., Willis, A. G., and Scott, J. S. 1979, *Nature*, **281**, 437.
Pietrini, P., and Torricelli-Ciamponi, G. 1989, *Phys. Fluids*, in press.
Pouquet, A., Meneguzzi, M., and Frish, U. 1986, *Phys. Rev. Letters*, **33**, 4266.
Rechester, A. B., Rosenbluth, M. N., and White, R. B. 1979, *Phys. Rev. Letters*, **42**, 1247.
Saikia, D. J., Shastri, P., Cornwell, T. J., and Banhatti, D. G. 1983, *M.N.R.A.S.*, **203**, 53P.
Shebalin, J. V., Matthaeus, W. H., and Montgomery, D. 1983, *J. Plasma Phys.*, **29**, 525.
Skilling, J. 1975, *M.N.R.A.S.*, **172**, 557.
van Breugel, W. J. M. 1980, *Astr. Ap.*, **88**, 248.
———. 1982, *Astr. Ap.*, **110**, 225.
van Breugel, W. J. M., and Willis, A. G. 1981, *Astr. Ap.*, **96**, 332.
Willis, A. G., Storm, R. G., Bridle, A. H., and Fomalont, E. B. 1981, *Astr. Ap.*, **95**, 250.
Zimbardo, G., Veltri, P., and Malara, F. 1984, *J. Plasma Phys.*, **31**, 141.

EDVIGE CORBELLI: Osservatorio Astrofisico di Arcetri, Largo E. Fermi, 5, 50125 Firenze, Italy

PIERLUIGI VELTRI: Dipartimento di Fisica, Universita' della Calabria, 87036 Arcavacata di Rende, Italy